

Interaction-Induced Localization of an Impurity in a Trapped Bose Condensate

Ryan M. Kalas and D. Blume

Department of Physics and Astronomy, Washington State University, Pullman, Washington 99164-2814, USA

(Dated: December 1, 2005)

We study the ground state properties of a trapped Bose condensate with a neutral impurity. By varying the strength of the attractive atom-impurity interactions the degree of localization of the impurity at the trap center can be controlled. As the impurity becomes more strongly localized the peak condensate density, which can be monitored experimentally, grows markedly. For strong enough attraction, the impurity can make the condensate unstable by strongly deforming the atom density in the neighborhood of the impurity. This “collapse” can possibly be investigated in bosonova-type experiments.

PACS numbers:

I. INTRODUCTION

The study of impurities immersed in liquids and solids has a long history. In 1933, Landau predicted, using quantum mechanical arguments, that the localization of electron impurities in a crystal could be used to probe the activation energy of solids [1]. Electron impurities have also played a key role in the study of liquids, in particular liquid ^4He [2]. More recently, the study of doped mesoscopic helium clusters has attracted much attention [3, 4]. Some atom impurities reside on the cluster surface while others migrate to the center of the helium cluster. Spectroscopic measurements of molecules located at the center of the cluster have, e.g., shown unambiguously that ^4He clusters with about 60 atoms are superfluid [5].

Recently, the study of impurities immersed in a gaseous, coherent atom background has become possible [6, 7]. Theoretical studies on, e.g., ion impurities in a condensate have been initiated [8, 9], raising questions about the appropriate treatment of systems with long-range interactions (unlike short-ranged atom-atom potentials, which behave as $1/r^6$ for large interparticle distances, atom-ion potentials fall off as $1/r^4$). Here, we consider a neutral impurity in an inhomogeneous Bose gas, assuming contact atom-impurity interactions [10]. Treatments for more complicated atom-impurity interactions exist [11, 12, 13]; the results may, however, be model-dependent. Our self-consistent mean-field treatment provides a first step towards a systematic understanding of impurities in a Bose condensate. We also discuss a simple variational treatment which reproduces the key features of the self-consistent results. We point towards possible experimental signatures of our predictions, which will be aided by the possibility of tuning the atom-atom and atom-impurity interactions in the vicinity of a Feshbach resonance by application of an external magnetic field [14, 15]. This tunability is unique to gaseous condensate-impurity systems; it does not, for example, exist in helium where the interaction strength is set by nature.

We consider a weakly-interacting Bose condensate in a harmonic trap, doped with a single impurity. For now, we assume that the impurity feels no external trapping

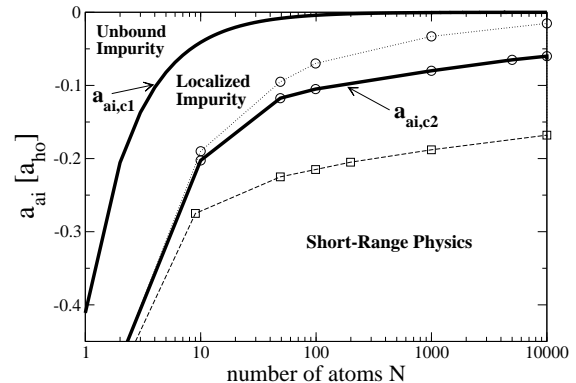


FIG. 1: Phase diagram for trapped Bose gas with a single impurity, which feels no confining potential, as a function of the number of atoms N and the atom-impurity scattering length a_{ai} for equal atom and impurity mass, i.e., $m_i = m_a$. The phase diagram contains three regions: in region (A) the impurity is unbound; in region (B) the impurity is localized (the localization is “weak” for comparatively small $|a_{ai}|$ and “strong” for comparatively large $|a_{ai}|$, see Sec. II for details); and in region (C) short-ranged physics becomes relevant. Regions (A) and (B) are separated by a critical value $a_{ai,c1}$ (upper bold solid line), which is approximately independent of a_{aa} . Regions (B) and (C) are separated by a critical value $a_{ai,c2}$, which is shown for $a_{aa} = 0.005a_{ho}$ (lower bold solid line), $a_{aa} = 0$ (dotted line), and $a_{aa} = 0.05a_{ho}$ (dashed line).

potential; later, we discuss how the presence of an impurity trapping potential modifies the results. Figure 1 shows the equilibrium “phase diagram” [16] determined within mean-field theory as a function of the number of atoms N and the atom-impurity scattering length a_{ai} . The phase diagram separates into three distinct regions: (A) For $a_{ai} > a_{ai,c1}$, the impurity is unbound and can move away from the trapped atom cloud. (B) For $a_{ai,c1} > a_{ai} > a_{ai,c2}$, the impurity is localized, i.e., bound to the atom cloud [17]. (C) For $a_{ai} < a_{ai,c2}$, short-range physics, which cannot be described within mean-field theory, becomes relevant. Regions (A) and (B) are separated by a N -dependent critical value $a_{ai,c1}$ (upper solid bold line in Fig. 1), which is approximately independent of the atom-atom scattering length a_{aa} . Since the impurity

feels no trapping potential, interaction-induced localization of the impurity occurs only if a_{ai} is more attractive than $a_{ai,c1}$. Regions (B) and (C) are separated by a N -dependent critical value $a_{ai,c2}$, which also depends on the atom-atom scattering length a_{aa} . The lower bold solid line in Fig. 1 shows $a_{ai,c2}$ for $a_{aa} = 0.005a_{ho}$, the dotted line that for $a_{aa} = 0$, and the dashed line that for $a_{aa} = 0.05a_{ho}$. If a_{ai} is more negative than $a_{ai,c2}$, the attractive atom-impurity interactions can “collapse” the condensate, pulling atoms into a short-ranged state about the impurity.

The next section outlines the self-consistent mean-field treatment used to calculate the phase diagram shown in Fig. 1. Section III develops a simple variational framework, which reproduces the key features of the full self-consistent mean-field treatment. Finally, Sec. IV discusses possible experimental realizations of the systems under study and concludes.

II. SELF-CONSISTENT MEAN-FIELD TREATMENT

We describe N atoms of mass m_a in the presence of a harmonic trapping potential with angular frequency ω_{ho} and a single impurity of mass m_i , which feels no external potential, within mean-field theory. Assuming that the atom-atom and atom-impurity interactions can be described by contact potentials, the many-body Hamiltonian reads

$$H = \sum_{j=1}^N \left[-\frac{\hbar^2}{2m_a} \nabla_j^2 + \frac{1}{2} m_a \omega_{ho}^2 \vec{x}_j^2 \right] - \frac{\hbar^2}{2m_i} \nabla_i^2 + U_{aa} \sum_{j < k}^N \delta(\vec{x}_j - \vec{x}_k) + U_{ai} \sum_{j=1}^N \delta(\vec{x}_j - \vec{x}_i), \quad (1)$$

where $U_{qp} = 2\pi\hbar^2 a_{qp}/m_{qp}$, $m_{qp} = m_q m_p / (m_q + m_p)$, and $(q, p) = (a, a)$ or (a, i) . In Eq. (1), \vec{x}_j and \vec{x}_i denote the position vectors of the j th atom and the impurity, respectively. We approximate the ground state wave function Φ as a product of single-particle wavefunctions,

$$\Phi(\vec{x}_1, \vec{x}_2, \dots, \vec{x}_N; \vec{x}_i) = \left[\prod_{j=1}^N \psi_a(\vec{x}_j) \right] \psi_i(\vec{x}_i), \quad (2)$$

and derive a set of coupled Hartree-Fock equations,

$$\left[-\frac{1}{2} \frac{\partial^2}{\partial r^2} + \frac{1}{2} r^2 + (N-1) \frac{a_{aa}}{a_{ho}} \frac{|\chi_a(r)|^2}{r^2} + \frac{a_{ai}}{a_{ho}} \frac{m_a}{2m_{ai}} \frac{|\chi_i(r)|^2}{r^2} \right] \chi_a(r) = \epsilon_a \chi_a(r) \quad (3)$$

and

$$\left[-\frac{1}{2} \frac{m_a}{m_i} \frac{\partial^2}{\partial r^2} + N \frac{a_{ai}}{a_{ho}} \frac{m_a}{2m_{ai}} \frac{|\chi_a(r)|^2}{r^2} \right] \chi_i(r) = \epsilon_i \chi_i(r). \quad (4)$$

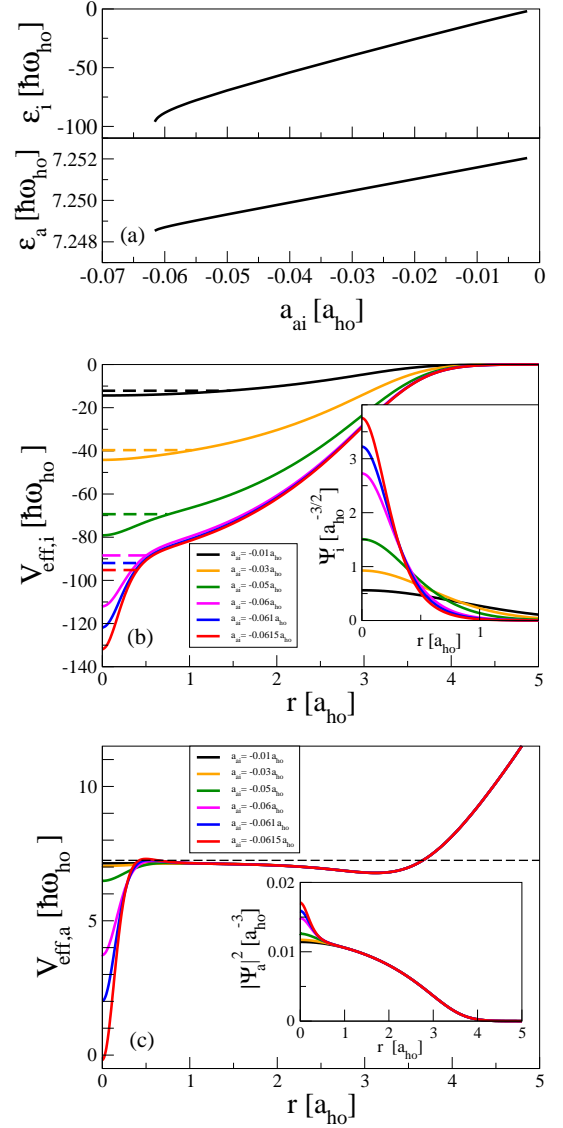


FIG. 2: (color online) Self-consistent mean-field results obtained for attractive atom-impurity interactions, $N = 10^4$, $a_{aa} = 0.005a_{ho}$, and $m_i = m_a$. Panel (a) shows the chemical potentials ϵ_i and ϵ_a as a function of a_{ai} . Solid lines in panels (b) and (c) show the effective potentials $V_{eff,i}(r)$ and $V_{eff,a}(r)$, respectively, for a few selected atom-impurity scattering lengths (see legend). Dashed lines show the corresponding chemical potentials [note that the change of ϵ_a is not visible on the scale chosen in panel (c)]. The insets of panels (b) and (c) show the corresponding impurity wave function $\psi_i(r)$ and atom density $|\psi_a(r)|^2$, respectively. The critical values $a_{ai,c1}$ and $a_{ai,c2}$ of this system are $\approx -4 \times 10^{-5}a_{ho}$ and $-0.062a_{ho}$, respectively.

Here, a_{ho} denotes the oscillator length ($a_{ho} = \sqrt{\hbar/m_a\omega_{ho}}$ and $\vec{r} = a_{ho}\vec{x}$), and ϵ_a and ϵ_i the chemical potentials (or “orbital energies”) of the atoms and the impurity. The coupled mean-field equations are equivalent to those for a two-component condensate [18] if one replaces one of the two components by a single impurity. In writ-

ing Eqs. (3) and (4), we have implied spherical symmetry, $\psi_{a,i}(\vec{r}) = \psi_{a,i}(r) = \frac{\chi_{a,i}(r)}{\sqrt{4\pi r}}$ with $\int_0^\infty |\chi_{a,i}(r)|^2 dr = 1$. For repulsive atom-impurity interactions, not considered here, symmetry-breaking states can exist [19].

The impurity feels an effective potential $V_{eff,i}$ [defined as the second term in square brackets on the left hand side (LHS) of Eq. (4)], which is created by the atom density $|\psi_a|^2$. The impurity density $|\psi_i|^2$ enters Eq. (3) and creates, together with the trapping potential and the atom density itself, an effective potential $V_{eff,a}$ [defined as the last three terms in square brackets on the LHS of Eq. (3)]. For weak atom-impurity interactions, the condensate atoms act to a good approximation as a static background with which the impurity interacts. However, as the strength of the atom-impurity interactions increases the full coupled nature of Eqs. (3) and (4) becomes important.

We discuss the self-consistent solutions to Eqs. (3) and (4), obtained by numerical means, for a specific set of parameters. The behavior is qualitatively similar for other parameters. Figure 2(a) shows the chemical potentials ϵ_i and ϵ_a as a function of a_{ai} for $N = 10^4$ and $a_{aa} = 0.005a_{ho}$, and $m_i = m_a$. Equal atom and impurity masses can be realized experimentally by, e.g., promoting a single condensate atom to a different hyperfine state [6]. Figure 2(a) shows that the chemical potentials ϵ_i and ϵ_a change approximately linearly with the atom-impurity scattering length for $-0.005 \gtrsim a_{ai}/a_{ho} \gtrsim -0.05$. This linear behavior is what one would expect from a perturbative treatment. To visualize the system's behavior, Figs. 2(b) and (c) show the effective potentials $V_{eff,i}(r)$ and $V_{eff,a}(r)$ for a few selected atom-impurity scattering lengths. Figure 2(b) shows that $V_{eff,i}$ becomes deeper as a_{ai}/a_{ho} goes from -0.01 to -0.03 to -0.05 . Accordingly, the impurity wave functions ψ_i , shown in the inset of Fig. 2(b), become more localized as $|a_{ai}|$ increases. Although $|\psi_i|^2$ changes significantly as a_{ai}/a_{ho} goes from -0.01 to -0.05 , $V_{eff,a}$ and $|\psi_a|^2$ change only slightly [see Fig. 2(c)].

For $a_{ai}/a_{ho} \lesssim -0.05$, the impurity chemical potential ϵ_i (and, to a lesser degree, the atom chemical potential ϵ_a) changes in a non-linear, i.e., non-perturbative, fashion. For the parameters at play here, this defines the regime of strong atom-impurity coupling. To highlight the dramatic changes of the system in this strongly-coupled regime, Figs. 2(b) and (c) show self-consistent effective potentials for three nearly identical atom-impurity scattering lengths, i.e., $a_{ai}/a_{ho} = -0.06, -0.061, -0.0615$. The peak impurity density grows with increasing $|a_{ai}|$ and creates a ‘‘hole’’ at the center of $V_{eff,a}$, which in turn causes the atom density to grow a ‘‘bump’’ at the trap center [see inset of Fig. 2(c)] with a length scale of roughly the condensate healing length ξ . The healing length is given by the competition between the kinetic energy and the condensate's mean-field energy, $\xi = 1/\sqrt{8\pi\rho_a a_{aa}}$ [20], where ρ_a denotes the peak density of the atoms, $\rho_a = N|\psi_a(r=0)|^2$. For the parameters of Fig. 2, $\xi \approx 0.26a_{ho}$. Since the healing

length ξ is the scale over which the condensate ‘‘reacts’’ to spatial perturbations, it is natural that the atom density develops a variation near the trap center of size ξ .

The inset of Fig. 2(c) illustrates the peak atom density growth with increasing $|a_{ai}|$. To quantify this growth, we calculate the excess number of atoms ΔN associated with the bump of the atom density. In analogy to a homogeneous system [9], we define ΔN as

$$\Delta N = 4\pi N \int_0^{r_c} [|\psi_a^{a_{ai} \neq 0}(r)|^2 - |\psi_a^{a_{ai} = 0}(r)|^2] r^2 dr, \quad (5)$$

where the atom wave function $\psi_a^{a_{ai} \neq 0}(r)$ is calculated self-consistently for a Bose gas with finite atom-impurity scattering length and $\psi_a^{a_{ai} = 0}(r)$ for a Bose gas with vanishing atom-impurity scattering length (for the same N and m_a). When evaluating Eq. (5) for a specific system, we choose the cutoff radius r_c to roughly coincide with the r -value at which the bump of the atom density starts growing. Triangles in Fig. 3 show the resulting number of excess atoms ΔN for $N = 10^4$, $m_i = m_a$, $a_{aa} = 0.005a_{ho}$ (the same parameters as in Fig. 2) and $r_c = 1a_{ho}$ for different values of the atom-impurity scattering length a_{ai} . The number of excess atoms increases roughly linearly with increasing $|a_{ai}|$. Just before the onset of instability at $a_{ai,c2} \approx -0.062a_{ho}$, the number of excess atoms ΔN reaches 12, which corresponds to 0.12 % of the total number of atoms. For comparison, a dashed line in Fig. 3 shows an estimate for the number of excess atoms derived for a weakly-interacting impurity-doped homogeneous Bose gas [9],

$$\Delta N = -\frac{m_{aa} a_{ai}}{m_{ai} a_{aa}}. \quad (6)$$

Figure 3 shows good agreement between the number of excess atoms ΔN calculated for the inhomogeneous impurity-doped condensate (triangles) and the analytical expression, Eq. (6). This suggests that Eq. (6) describes the number of excess atoms for large enough, weakly-interacting inhomogeneous condensates quite accurately.

Finally, if a_{ai} becomes more negative than a critical value of $a_{ai,c2} \approx -0.062a_{ho}$, we no longer find a self-consistent solution to Eqs. (3) and (4). This implies that the condensate collapses, i.e., atoms are drawn into a short-ranged state about the impurity. It appears likely that this collapse involves only a fraction of the condensate atoms, but a definite answer lies beyond the scope of the present work. Just as in the case of pure atomic condensates with negative atom-atom scattering length, mean-field theory predicts the onset of collapse for our coupled equations but cannot describe the system's behavior in the regime dominated by short-range physics.

We now estimate the critical value $a_{ai,c1}$, which separates the unbound impurity phase from the localized impurity phase for $m_i = m_a$ (see upper bold solid line in Fig. 1). The impurity feels a strictly short-ranged potential, i.e., $V_{eff,i}(r)$ falls off faster than a power-law of r . Since the impurity equation, Eq. (4), is linear, we can compare the volume-integrated strength of

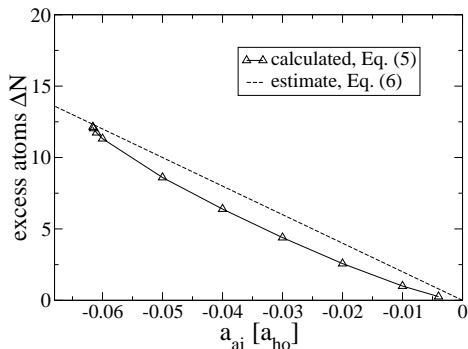


FIG. 3: Triangles show the number of excess atoms ΔN calculated from Eq. (5) using the self-consistent mean-field solutions for $N = 10^4$, $a_{aa} = 0.005a_{ho}$ and $m_a = m_i$ (the same parameters as in Fig. 2), as a function of the atom-impurity scattering length a_{ai} . For comparison, a dashed line shows the analytical estimate, Eq. (6).

$V_{eff,i}$ with the corresponding critical value, $-\frac{\pi^3 \hbar^2 b}{6 m_i}$ [21], for forming a bound state in three dimensions in a potential of range b . If we identify the range b with a_{ho} , we find that the critical value of a_{ai} scales as $1/N$, i.e., $a_{ai,c1}(N)/a_{ho} = -\frac{\pi^2}{24N} \approx -\frac{0.411}{N}$. For positive a_{aa} , the atom cloud is somewhat larger, and our estimate will be off by a numerical factor of order 1. The upper bold solid line in Fig. 1 shows our analytical estimate. The results of our numerical calculations are consistent with this analytical estimate. The critical value $a_{ai,c1}$ might be difficult to observe experimentally since the transition from region (A) to region (B) involves a diverging length scale. Furthermore, it might be difficult to experimentally realize a trapping setup with tunable atom-impurity scattering length a_{ai} for which the impurity feels no confining potential (see also Sec. IV).

The behavior of the impurity-doped condensate was illustrated in Fig. 2 for $N = 10^4$ atoms. We find similar qualitative features for a smaller number of atoms, including the disappearance of the mean-field solutions. The critical values $a_{ai,c1}$ and $a_{ai,c2}$ vary with N as shown in Fig. 1. We note that the notion of a condensate healing length, and thus the discussion of the disappearance of the mean-field solution at the point when the impurity becomes more tightly localized than this scale, becomes less meaningful for small enough number of atoms. It will be interesting to further investigate the properties of an impurity immersed in a small condensate since such systems can be realized experimentally with the aid of optical lattices.

III. VARIATIONAL TREATMENT

To further illustrate how the neutral impurity alters the atom cloud, we minimize the total energy variationally for the Hamiltonian given in Eq. (1) and the wave

function given in Eq. (2) with

$$\psi_i \propto e^{-p_i r^2}, \quad \text{and} \quad \psi_a \propto (e^{-p_a r^2} + c e^{-p_b r^2}). \quad (7)$$

The variational parameters p_i and p_a determine respectively the width of the impurity and of the atom wave function. To be able to describe the growth of the atom peak density in the strongly-interacting regime and the collapse of the condensate, ψ_a contains an additional gaussian with two more variational parameters, the relative amplitude c and parameter p_b . We restrict p_b to be greater than p_a to separate the background condensate cloud from the more localized condensate bump.

Figure 4 shows the results of our variational calculations for $N = 10^4$, $a_{aa} = 0$, and $m_i = m_a$ as a function of a_{ai} . To reduce the parameter space we set $p_a = 0.5a_{ho}^{-2}$; we checked that allowing p_a to vary changes its value only little. The optimal values of the remaining three variational parameters p_i , p_b and c are shown in panels (c) and (d) of Fig. 4 by triangles, and the corresponding chemical potentials of the impurity and atom, respectively, are shown in panels (a) and (b) by triangles. The variational analysis predicts a critical value of $a_{ai,c2} \approx -0.020a_{ho}$; at this critical value $a_{ai,c2}$, the local minimum in the variational energy disappears as the variational energy becomes unbounded from below. For comparison, our self-consistent solutions to Eqs. (3) and (4), which are shown in panels (a) and (b) by circles for comparison, predict a somewhat less attractive critical value, i.e., $a_{ai,c2} \approx -0.016a_{ho}$. This is to be expected since the self-consistent total energy (not shown) provides a better lower bound than the variational energy. The variational parameters p_i , p_b and c shown in panels (c) and (d) of Fig. 4 nicely illustrate the degree of impurity localization. For small $|a_{ai}|$, the amplitude c is negligible, indicating that the presence of the impurity barely affects the condensate. As $|a_{ai}|$ increases, the impurity becomes more tightly localized, i.e., p_i increases (note that the width of the impurity density scales as $1/\sqrt{p_i}$), which in turn drives the growth and localization of the condensate bump, i.e., c and p_b also increase. Since p_i drives the increase of p_b , p_b necessarily increases slower than p_i with increasing $|a_{ai}|$.

To connect our results for the variational parameter c with the full self-consistent solutions, we fit our solutions to Eqs. (3) and (4) to the wavefunctions of Eq. (7) with the proper normalization, treating p_i , p_b , and c as fitting parameters. The circles plotted in Fig. 4(d) show the resulting values of c extracted from the self-consistent solution. To a very good approximation, c^2 describes the percentage change in the peak condensate density for the system with non-vanishing a_{ai} as compared to the system with vanishing a_{ai} (assuming we keep a_{aa} and the number of atoms N fixed). Figure 4(d) shows that, just before collapse at $a_{ai,c2}$, $c \approx 0.53$ for the full self-consistent solution to Eqs. (3) and (4) and $c \approx 0.68$ for the variational solution. These values of c correspond to changes in the peak condensate density, as compared to the condensate without impurity, of greater than 25%. We note that a

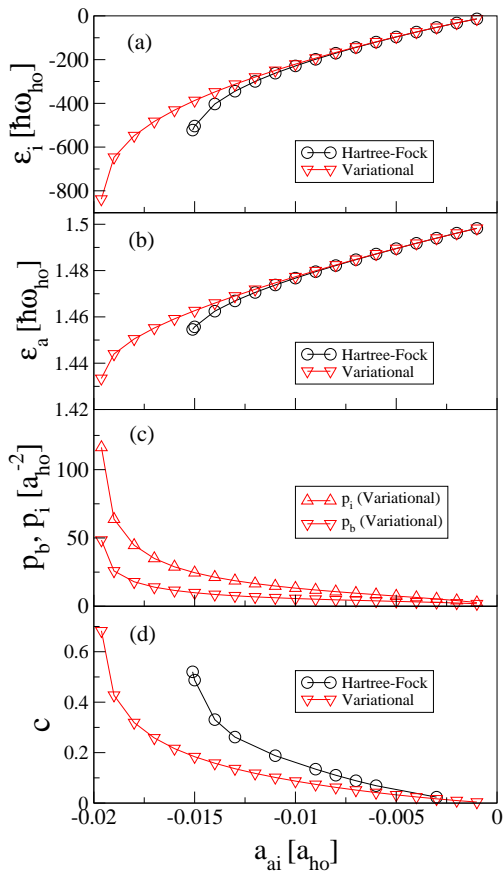


FIG. 4: (color online) Triangles show the chemical potentials ϵ_i and ϵ_a [panels (a) and (b)], and the parameters p_b , p_i and c [panels (c) and (d)] for $N = 10^4$, $a_{aa} = 0$ and $m_i = m_a$ as a function of a_{ai} , obtained from the variational treatment. For comparison, circles in panels (a) and (b) show ϵ_i and ϵ_a , and those in panel (d) the parameter c obtained by fitting the self-consistent solutions of Eqs. (3) and (4) (see text).

similar growth of the peak condensate density is seen in the inset of Fig. 2(c) for the same number of atoms, i.e., $N = 10^4$, but non-vanishing atom-atom interactions, i.e., $a_{aa} = 0.05a_{ho}$.

The variational wavefunction given in Eq. (7) is best-suited to describe the case of $a_{aa} = 0$. For $a_{aa} \neq 0$ the atom cloud deviates from a gaussian, and for strong enough interactions a gaussian form for the atom cloud is a poor approximation. Consequently, as the atom-atom interactions increase, we find that the simplistic variational wave function given in Eq. (7) cannot describe the tightly-localized impurity at the trap center prior to the onset of collapse. Nonetheless, for the case $a_{aa} = 0$ discussed above, the variational treatment reproduces the key features of the full self-consistent solution and provides us with further insights. In particular, the form of the variational wavefunction, Eq. (7), is useful in visualizing how the condensate develops features characterized by a length scale much smaller than the oscillator length. Furthermore, the disappearance of the local minimum as

the variational energy becomes unbounded from below is another indication, along with the disappearance of the self-consistent solutions, of the collapse of the condensate.

IV. DISCUSSION AND CONCLUSION

Sections II and III discuss the behaviors of a single neutral impurity, which feels no external confining potential, immersed in a trapped condensate. If the impurity feels an external trapping potential with angular frequency ω_i , which might be the case in an experiment (see below), region (A) in Fig. 1 is absent, i.e., the impurity is always localized due to the presence of the external potential. Assuming that the impurity trapping potential has a characteristic length which is larger than roughly the condensate healing length (for large enough number of atoms), the comparatively strong impurity localization prior to collapse and the crossover from region (B) to region (C) in Fig. 1 are, however, nearly unaltered. For example, for $N = 10^4$, $a_{aa} = 0.005a_{ho}$, $m_i = m_a$ and $\omega_a = \omega_i$, the onset of collapse occurs at the same critical value of $a_{ai,c2} \approx -0.062a_{ho}$ that we find without impurity trap.

Impurity-doped condensates can be realized experimentally with present-day technology [6]. If one considers a magnetically trapped condensate, an impurity can, e.g., be created by promoting one of the condensate atoms to a different hyperfine state. The promoted atom may or may not feel the magnetic confinement. Alternatively, one could implant a different atom, magnetic or non-magnetic, into the cloud. Such systems have the disadvantage that the atom-impurity interactions cannot be tuned via a magnetic Feshbach resonance. To take advantage of the tunability of interspecies scattering lengths [22], one can consider an optical potential red-detuned with respect to the atoms and the impurity. In such an experimental realization both the atom and the impurity would feel trapping potentials.

As the atom-impurity interactions are tuned closer to $a_{ai,c2}$, the growth of the peak atom density at the center of the trap can potentially be monitored experimentally in expansion experiments. Since the condensate bump at the trap center involves only a few atoms, direct detection of the changes in the peak density may, however, be non-trivial. We suggest that the impurity-doped condensate could alternatively be probed in a bosonova-type experiment which applies a sequence of time-dependent magnetic field ramps [23]. By tuning the atom-impurity scattering length to a large negative value, one could experimentally induce collapse and consequently density oscillations, which might involve a significant fraction of the condensate atoms.

A key result of our study is that the degree of localization of the impurity at the trap center in region (B) of the phase diagram (see Figs. 1 and 2) can be controlled by varying the atom-impurity scattering length, i.e., the

width of the impurity wave function for a system with $m_a = m_i$ can be varied from a size much greater than the oscillator length a_{ho} to a size significantly smaller than a_{ho} . In addition to changing the atom-impurity scattering length, one can consider unequal atom and impurity masses, e.g., a Cs atom immersed in a Na condensate. Not surprisingly, as the impurity mass increases, the degree of impurity localization also increases. The localized impurity itself may present the possibility for forming interesting single-atom devices, perhaps using the impurity's spin degrees of freedom. The favorable coherence properties of Bose condensates may make the localized impurity states viable for quantum computing schemes. Furthermore, extensions to two or more impurities will allow one to consider the role of condensate-mediated in-

teractions between impurities.

Finally, we return to our finding that a single neutral impurity can deform the condensate sufficiently to induce a collapse which may only involve a fraction of the condensate atoms. The resulting collapsed state may be related to the mesoscopic droplets that have been predicted to form about an ion immersed in a condensate [8]. More work is needed to fully understand these ion states, the collapsed states predicted in the present work, and possible connections between the two.

We gratefully acknowledge fruitful discussions with A. Bulgac, M. Davis, P. Engels, B. Esry and, E. Timmermans, hospitality of the Institute for Nuclear Theory at the University of Washington, and support by the NSF, grant PHY-0331529.

-
- [1] L. Landau, Phys. Z. Sowjetunion **3**, 664 (1933).
 [2] J. P. Hernandez, Rev. Mod. Phys **63**, 675 (1991).
 [3] J. P. Toennies, A. V. Vilesov, and K. B. Whaley, Phys. Today **54**, 31 (2001).
 [4] C. Callegari, K. K. Lehmann, R. Schmieid and G. Scoles, J. Chem. Phys. **115**, 10090 (2001).
 [5] S. Grebenev, J. P. Toennies and A. F. Vilesov, Science **279**, 2083 (1998).
 [6] A. P. Chikkatur, A. Görlitz, D. M. Stamper-Kurn, S. Inouye, S. Gupta, and W. Ketterle, Phys. Rev. Lett. **85**, 483 (2000).
 [7] D. Ciampini, M. Anderlini, J. H. Müller, F. Fuso, O. Morsch, J. W. Thomsen, and E. Arimondo, Phys. Rev. A **66**, 043409 (2002).
 [8] R. Coté, V. Kharchenko, and M. D. Lukin, Phys. Rev. Lett. **89**, 093001 (2002).
 [9] P. Massignan, C. J. Pethick, and H. Smith, Phys. Rev. A **71**, 023606 (2005).
 [10] Neutral impurities in homogeneous Bose gases with delta function interactions have been considered by linearizing the atom equation, with extensions to inhomogeneous gases within the Thomas-Fermi approximation. E. Timmermans, talk at DAMOP, Lincoln, NE, May 19, 2005, and F. Cucchietti and E. Timmermans, unpublished.
 [11] P. Capuzzi, E. S. Hernández, and M. Barranco, Phys. Rev. A **62**, 023603 (2000).
 [12] P. Navez, and M. Wilkens, J. Phys. B **32**, L629 (1999).
 [13] S. A. Chin and H. A. Forbert, cond-mat/9901028; Physica B **284-288**, 13 (2000); Phys. Lett. A **272**, 402 (2000).
 [14] S. Inouye, M. R. Andrews, J. Stenger, H. J. Miesner, D. M. Stamper-Kurn, and W. Ketterle, Nature **392**, 151 (1998).
 [15] S. L. Cornish, N. R. Claussen, J. L. Roberts, E. A. Cornell, and C. E. Wieman, Phys. Rev. Lett. **85**, 1795 (2000).
 [16] The transition from unbound to localized impurity is associated with a diverging length scale, i.e., it is a localization transition. The transition from the localized impurity to short-range physics is to be taken figuratively; the critical line $a_{ai,c2}(N)$ indicates a change of behavior of the system whose description goes beyond mean-field theory, as discussed further in the text.
 [17] Throughout this paper, a localized impurity is characterized by a negative chemical potential ϵ_i of the impurity. An unbound impurity has a positive chemical potential.
 [18] B. D. Esry, C. H. Greene, J. P. Burke, Jr., and J. L. Bohn, Phys. Rev. Lett. **78**, 3594 (1997). H. Pu and N. P. Bigelow, Phys. Rev. Lett. **80**, 1130 (1998).
 [19] C. K. Law, H. Pu, N. P. Bigelow, and J. H. Eberly, Phys. Rev. Lett. **79**, 3105 (1997). B. D. Esry, Phys. Rev. A **58**, R3399 (1998). B. D. Esry and C. H. Greene, Phys. Rev. A **59**, 1457 (1999).
 [20] F. Dalfovo, S. Giorgini, L. P. Pitaevskii and S. Stringari, Rev. Mod. Phys. **71**, 463 (1999).
 [21] L. D. Landau and E. M. Lifshitz, *Quantum Mechanics* (Butterworth-Heinemann, 2000), Sections 33 and 45.
 [22] S. Inouye, J. Goldwin, M. L. Olsen, C. Ticknor, J. L. Bohn, and D. S. Jin, Phys. Rev. Lett. **93**, 183201 (2004).
 [23] E. A. Donley, N. R. Claussen, S. L. Cornish, J. L. Roberts, E. A. Cornell, and C. E. Wieman, Nature **412**, 295 (2001).